Fragmentation of Energy-Selected Fluorobenzene Ion

Toshihide NISHIMURA,* Gerry G. MEISELS,† and Yoshio NIWA††
Upjohn Pharmaceuticals Limited, Tsukuba Research Laboratories, 23 Wadai, Tsukuba, Ibaraki 300-42
†Office of the Provost, University of South Florida, Tampa FL 33620, U.S.A.
††National Chemical Laboratories for Industry, Yatabe, Tsukuba, Ibaraki 305
(Received May 15, 1991)

Dissociation of the fluorobenzene ion has been studied using threshold photoelectron–photoion coincidence (TPEPICO) mass spectrometry. The detailed breakdown curves were measured over internal energies from 0 to 9 eV. Asymmetric flight time distributions due to metastable dissociation were observed for the formations of $C_6H_5^+$ and $C_4H_3F^+$, and their absolute decay rate constants were derived from their flight time distributions. The information-theoretical approach has been employed for the analysis of kinetic energy release distribution (KERD). The results of surprisal analysis demonstrated that experimental KERDs are in good agreement with the predictions based on the statistical theory of mass spectra (QET). The heat of formation of $C_4H_3F^{\cdot+}$ has been estimated to be 222±2 kcal mol^{-1}.

The quasi-equilibrium theory (QET)[1,2] on the unimolecular dissociation of gaseous ions assumes that (1) initial vibronic excitation by ionization is converted rapidly to vibrational energy of the ground electronic state of the molecular ion, that (2) all internal modes are accessible at a given total energy and vibrational energy redistribution within an energized molecular ion is much faster than dissociation (RRKM theory);[3,4]

$$k_d \ll k_{IC} \text{ and } k_{rdt}. \tag{1}$$

Here, k_d, k_{IC}, and k_{rdt} are respectively the rate constants of dissociation, internal conversion and redistribution of initial internal energy. Furthermore, QET requires (3) an equilibrium between the molecular ion M^+ and the transition state $T^{+\neq}$:

$$M^+ \underset{k_{-1}}{\overset{k_1}{\rightleftarrows}} T^{+\neq} \xrightarrow{k_d} \text{fragment ion} + \text{neutrals} \tag{2a}$$

and

$$k_1 \text{ and } k_{-1} \gg k_d. \tag{2b}$$

These assumptions result in the following QET expression of decay rate constant:[1]

$$k(E) = \sigma \int_0^{E_i - E_a} \rho^{\neq}(E)\, dE/h\, \rho(E_i), \tag{3}$$

where $\rho(E_i)$ is the state density of the molecular ion with internal energy of E_i, $\rho^{\neq}(E)$ that of the transition state for the dissociation process with the activation energy E_a and σ the degeneracy of reaction pathways.

Energized diatomic and triatomic molecules often relax by state-specific dissociation and/or radiative transition (fluorescence, etc.).[5–7] When the molecular ion is sufficiently large, radiative transition usually does not compete with internal conversion because of its high density of states. Therefore, a large molecular ion characterized by a large phase space should satisfy these hypothesis[1–3] which the quasi-equilibrium theory assumes.

Molecular ions containing a fluorine atom were frequently reported to dissociate nonstatistically, which include CF_4^+ and $C_2F_6^+$.[5,6] In the case of CF_4^+ fluorescent transition plays an important role prior to dissociation.[5] Here we have studied dissociation of the fluorobenzene by using threshold photoelectron–photoion coincidence (TPEPICO) mass spectrometry[8,9] since this molecule is an example of large molecular size and also contains a heteroatom fluorine. Time-dependent breakdown curves[10,11] have also been derived from absolute decay rate constants obtained experimentally and the information-theoretical approach[12] has been employed to study energy disposal in fragmentation.

Experimental

Our TPEPICO mass spectrometer has been described in detail previously.[13,14] It was used under the double-field source and space focusing condition.[15–17] A typical field strength in an ionization region was 20.0 V cm^{-1}, and the corresponding energy resolution for threshold photoelectrons was about 21 meV (FWHM) for the Ar $^2P_{3/2}$ state. The TOF mass resolution ($T/2\Delta T$) was about 50 amu (FWHM) for thermal ions.

Breakdown curves were constructed from relative ion abundances obtained from TOF peak areas. Overlapped ion peaks were deconvoluted assuming that a TOF mass peak is Gaussian. Because the m/z 95 ion was not fully separated from those of the m/z 96 ion under the ion extraction field of 20 V cm^{-1}, their relative abundances were evaluated from deconvolution results of those TOF peaks measured under the 34 V cm^{-1} field strength corresponding to the mass resolution of about 70 amu (FWHM). Ion loss due to initial kinetic energy was not taken into account for construction of breakdown curves.

Fluorobenzene was commercially obtained from Aldrich with a stated purity of 99% and was used without further purification. Both HeI photoionization and 70 eV electron-impact ionization mass spectra measured by an Extranuclear 324-9 quadrupole mass spectrometer and a Kratos AEI MS-50 DA, respectively, showed no significant impurity. All experiments were carried out at a source pressure of 3×10^{-5} Torr (1 Torr=133.322 Pa) and at room temperature.

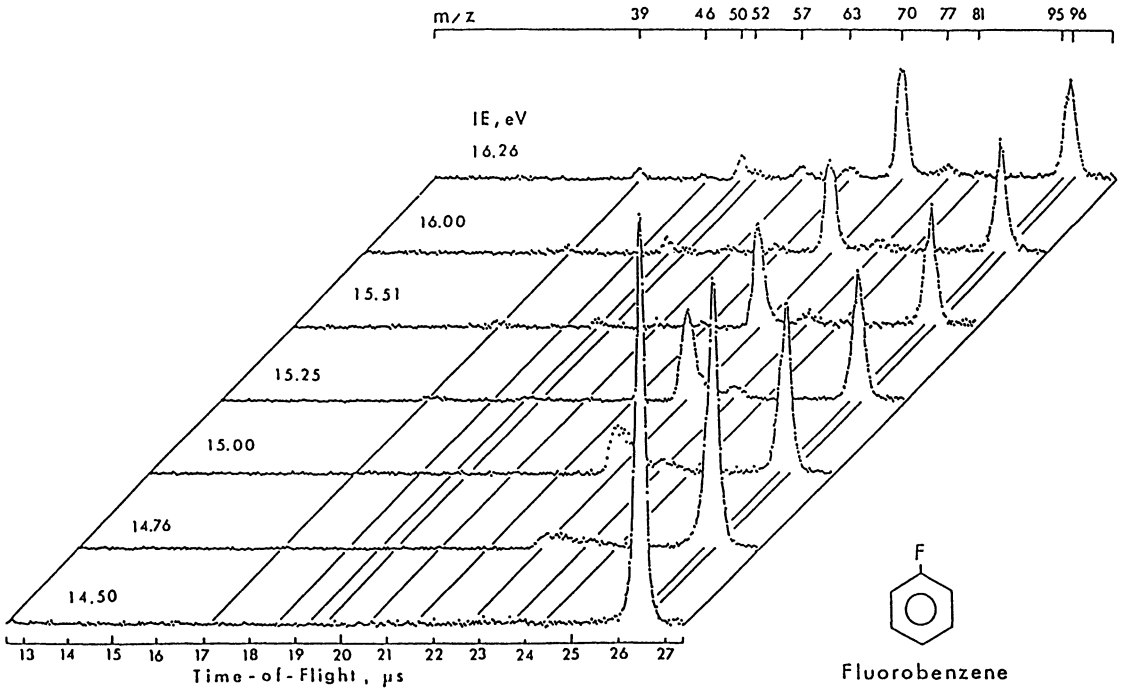

Fig. 1. Typical coincidence TOF mass spectra at several photon energies.

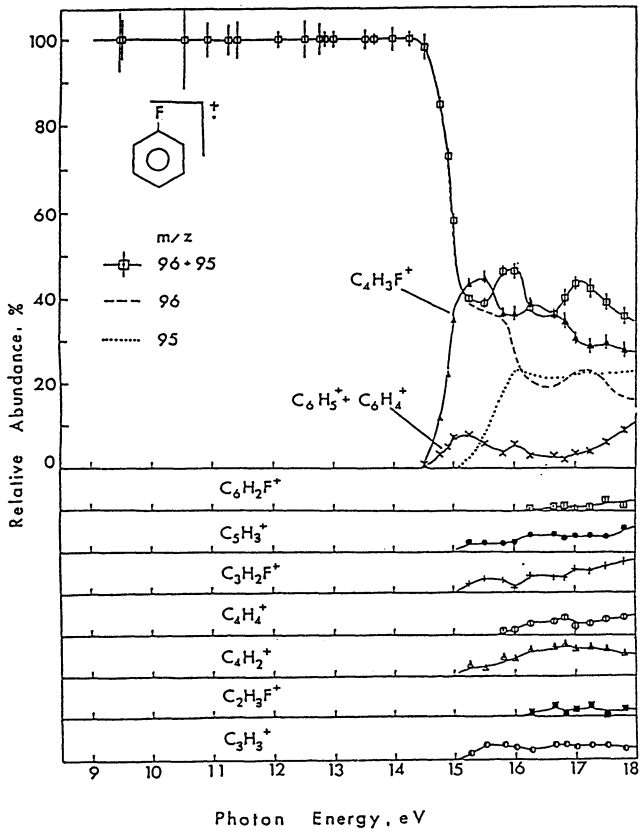

Fig. 2. The experimental breakdown curves of the fluorobenzene ion measured under an ion extraction field of 20 V cm^{-1}. The breakdown curve of $C_6H_4F^+$ was estimated from deconvolution of overlapped peaks of m/z 96 and 95 measured under the 34-V cm^{-1} extraction field, assuming the individual peaks are Gaussian.

Results and Discussion

Breakdown Curves and Fragmentation Pathways. Major products ions are $C_6H_5F^+$ (m/z 96), $C_6H_4F^+$ (m/z 95), $C_5H_2F^+$ (m/z 81), $C_6H_5^+$ (m/z 77), $C_6H_4^+$ (m/z 76), $C_4H_3F^+$ (m/z 70), $C_5H_3^+$ (m/z 63), $C_3H_2F^+$ (m/z 57), $C_4H_4^+$ (m/z 52), $C_4H_2^+$ (m/z 50), $C_2H_3F^+$ (m/z 46), and $C_3H_3^+$ (m/z 39). Fig. 1 shows typical coincidence TOF mass spectra measured at several photon energies, and the experimental breakdown curves are presented in Fig. 2. Fragmentation pathways elucidated from

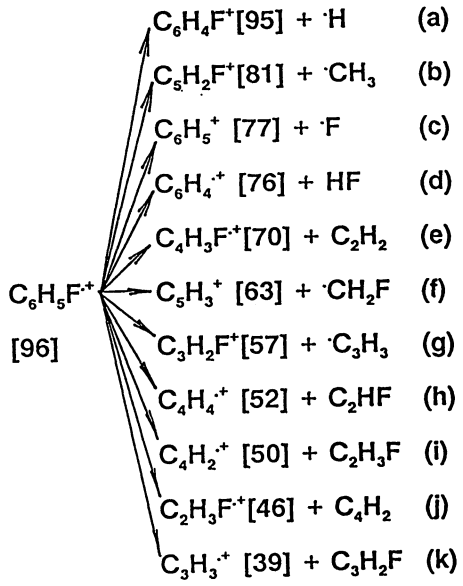

Fig. 3. Major fragmentation pathways of the fluorobenzene ion.

appearance potentials are summarized in Fig. 3. Appearance potentials obtained from breakdown curves are listed in Table 1. Among these dissociations abundant processes are (1) the C_2H_2-loss (Reaction e), (2) the hydrogen-loss (Reaction a) and (3) the fluorine elimination (Reaction c) from the molecular ion.

Table 1. Appearance Potentials (eV) for the Fragmentation Processes of Fluorobenzene Ion

m/z	Fragmentation process	Literature	This work
95	$C_6H_4F^+ + {}^{\cdot}H$	14.1[a]	
81	$C_5H_2F^+ + {}^{\cdot}CH_3$		16.13±0.13
77	$C_6H_5^+ + {}^{\cdot}F$	14.5±0.1[b]	13.10±0.05[e]
76	$C_6H_4^{\cdot+} + HF$	15.37±0.1[c]	
70	$C_4H_3F^{\cdot+} + C_2H_2$	14.73[d]	13.14±0.05[e]
63	$C_5H_3^+ + {}^{\cdot}CH_2F$		15.13±0.13
57	$C_3H_2F^+ + {}^{\cdot}C_3H_3$	15.77±0.1[c]	15.13±0.13
52	$C_4H_4^{\cdot+} + C_2HF$	17.00±0.1[c]	15.90±0.09
50	$C_4H_2^{\cdot+} + C_2H_3F$		15.13±0.13
46	$C_2H_3F^{\cdot+} + C_4H_2$		16.13±0.13
39	$C_3H_3^+ + {}^{\cdot}C_3H_2F$	14.27±0.1[c]	15.13±0.13

a) Ref. 28. b) Refs. 29 and 30. c) Ref. 31. d) Ref. 32. e) These values were adiabatic appearance potentials obtained by QET calculations (see text).

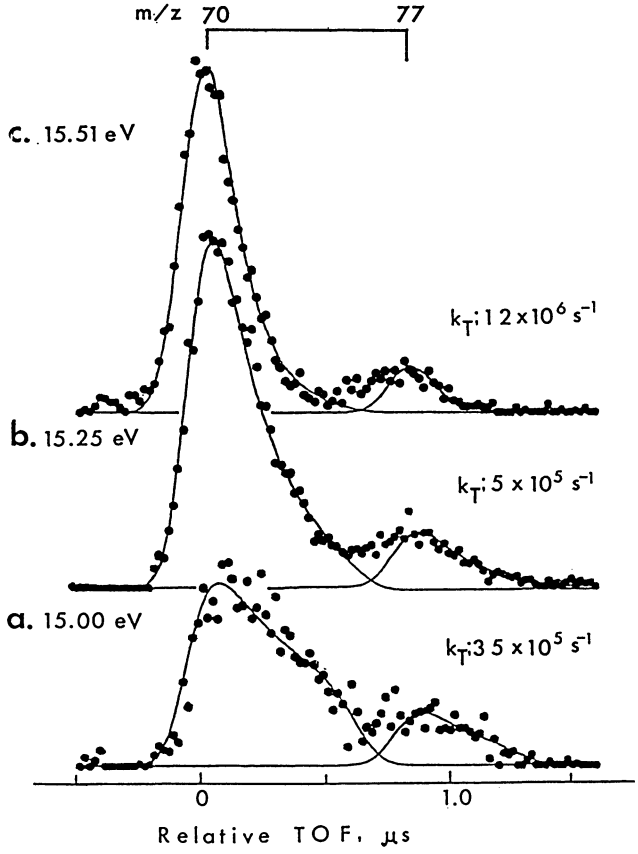

Fig. 4. The flight time distributions of m/z 70 and 77 ions (closed circles) observed at several photon energies under an ion extraction field of 34 V cm^{-1}. The solid curves are the distributions convoluted by the indicated decay rate constants.

Absolute Decay Rate Constants and Time-Dependent Breakdown Curves. A. Metastable Fragmentation. Asymmetric flight time distributions due to metastable dissociation[18] were observed for the C_2H_2- and F-eliminations from the parent ion which are formations of $C_6H_5^+$ and $C_4H_3F^+$ (Fig. 4). Total decay rate constants k_T were obtained directly from their asymmetric TOF distributions: Flight time distributions resulting from metastable fragmentation which occurs in both the first and second ion extraction fields were calculated numerically. The rate constant and initial ion kinetic energy were then adjusted until the calculated TOF distribution agrees with experiment. Experimental TOF distributions for both $C_6H_5^+$ and $C_4H_3F^+$ ions were found to be well fitted by using a single and same

Table 2. The Total Decay Rate Constants Observed for the Formations of $C_6H_5^+$ and $C_4H_3F^+$

Ionization energy (eV)	Total decay rate (×10^6 s^{-1})	
	$C_6H_5^+$	$C_4H_3F^+$
14.76	0.3±0.2	0.2±0.1
14.90	0.5±0.2	0.5±0.2
15.00	0.6±0.1	0.6±0.1
15.25	1.6±0.2	1.6±0.2
15.50	4±1	4±1

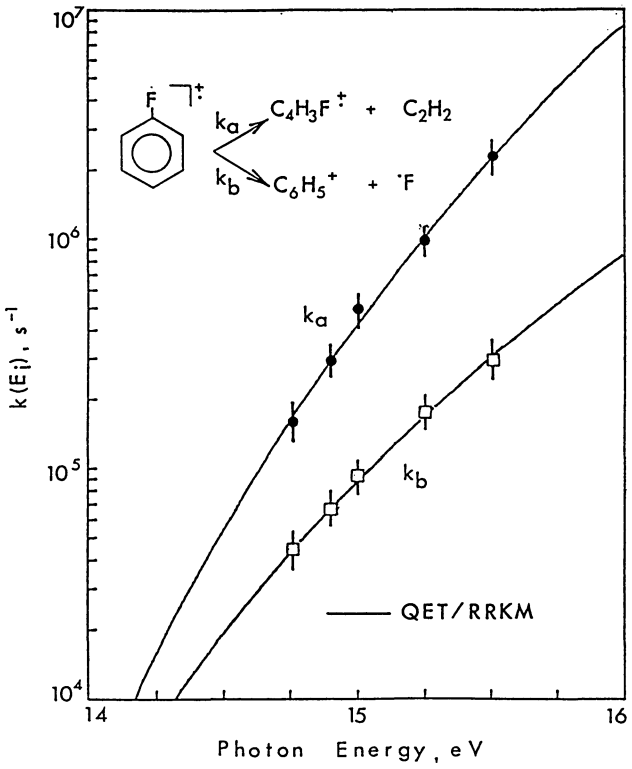

Fig. 5. Metastable decay rate constants for the formations of $C_4H_3F^+$ and $C_6H_5^+$ as a function of photon energy. Circles are the experimental decay rate constants. Solid curves are those obtained by QET calculations with the best fits to the experimental data.

rate constant (Table 2). Thus the same total rate observed suggests a competing dissociation mechanism for the fluorine and C_2H_2 loss channels. Individual rate constants for these reactions were therefore obtained from relative abundances in the breakdown diagram.

Individual decay rate constants are plotted against photon energy in Fig. 5 in comparison with those calculated by QET (the solid curves). In the QET calculation the vibrational frequencies of fluorobenzene ion were taken to be the same as those of the neutral molecule and the vibrational frequencies of the transition state were derived by multiplying those of the ion (excluding a reaction mode) by a factor F reflecting tightness ($F>1$) or looseness ($F<1$) of the transition state.[19] The frequencies and parameters used are listed in Table 3. The density of vibrational states were calculated using the Whitten-Rabinovitch approximation.[20] The activation energy E_a and factor F were used as adjustable parameters until the best fit to experiment is obtained.

Adiabatic appearance potentials were evaluated to be

Table 3. The Vibrational Frequencies Used in the QET Calculations.[a,b] The Number n in (n) Denotes the Degeneracy of Vibrational Frequency

3100	3090	3070	3050	3040	1600(2)
1500	1460	1330(2)	1220	1160(2)	1070
1020	1010	1000	970	900	820
810	750	690	610	520	500
410	400	240			

a) Ref. 33. b) For the formation of $C_4H_3F^+$, $C_6H_5^+$, and $C_6H_4F^+$ their reaction coordinates were assumed to be the ring breathing mode (1160 cm^{-1}) (F=0.9), the C–F stretching mode (1220 cm^{-1}) (F=1.1) and the C–H stretching mode (3040 cm^{-1}) (F=0.78), respectively.

respectively 13.10±0.05 eV and 13.14±0.05 eV for the formations of $C_6H_5^+$ and $C_4H_3F^+$, using the relation

$$AP_{adb} = IP + E_a, \quad (4)$$

Herein, the ionization potential IP of the fluorobenzene molecule was taken to be 9.11 eV from the literature.[27] Using these values the heat of formations $\Delta H_f(C_6H_5^+)$ and $\Delta H_f(C_4H_3F^+)$ were evaluated to be 257±2 and 222±2 kcal mol^{-1}. The heat of formation obtained in this work for the phenyl cation can be compared with the value ΔH_{f298}° ($C_6H_5^+$) of about 272 kcal mol^{-1} (1140 kJ mol^{-1}) suggested in Ref. 34 after rough correction of kinetic shift (50 kJ mol^{-1}).

B. Kinetic Shift. The experimental breakdown curves of the parent ion measured under the different field strengths of ion extraction (E_s=20 and 34 V cm^{-1}) shifted by ca. 0.1 eV. This shift results from difference in the reaction time equal to a time spending during acceleration in a TOF mass spectrometer, which are calculated to be 3.4 and 2.6 μs, respectively. The breakdown curves for these reaction times were reconstructed from the individual rate constants, and are presented in Fig. 6. In the figure a shift, about 75 meV, of crossover point between the breakdown curves of the parent ion and $C_4H_3F^+$ was consistent with experiment. The calculated breakdown curves are fairly in good agreement with the TPEPICO breakdown curves.

Such a kinetic shift leads to heat of formations higher than those derived from adiabatic potentials, and can be ascribed to a large phase space volume of the molecular ion brought about by (1) a large number of internal modes or a high density of states $\rho(E)$ and (2) a high activation energy E_a. A large phase space volume corresponds to a long lifetime of a fragmenting ion which is the average time until a given phase point crosses over the critical surface to dissociation. Our observations

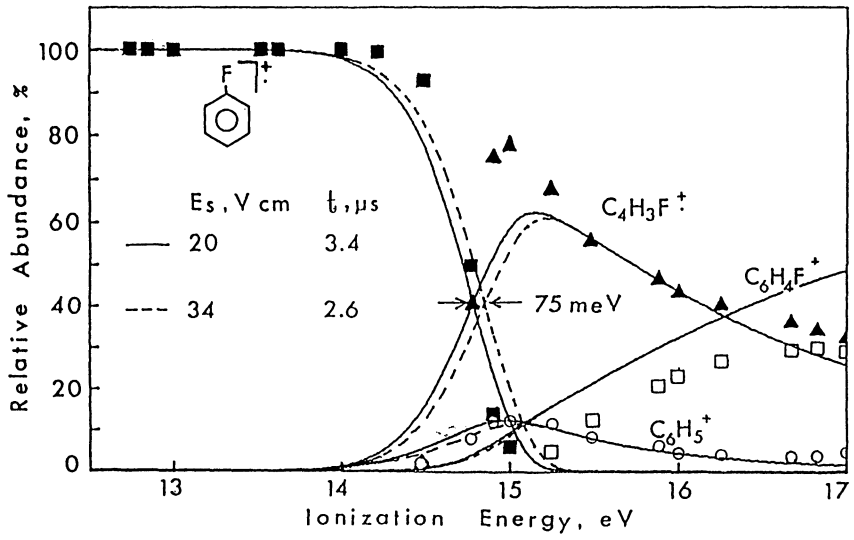

Fig. 6. The breakdown curves for the reaction times 3.4 and 2.6 μs corresponding to the extraction fields of 20 and 34 V cm^{-1}, respectively. Symbols are the corrected breakdown curves for the 20-V cm field.

are thus consistent with the prediction by QET.

Information-Theoretical Analysis of Energy Disposal in Fragmentation. A. Kinetic Energy Release Distribution (KERD). Kinetic energy release distributions for the formation of $C_4H_3F^+$ ions (m/z 70) were extracted from their flight time distributions using a linear regression method. The approach utilized here has been described previously, which follows those used by Powis et al.[21] and Baer et al.[22]

A typical deconvolution result is presented in Fig. 7. Here we used the minimum energy E_o=5.0 meV, the room temperature T=300 K and the nine discrete kinetic energy releases: $Q=(2n-1)^2 E_o$ (i=1 to 9). The experimental flight distribution $F(t)$ was convoluted by a series of calculated distributions $F(t; Q_i)$:

$$F(t)=\sum_i W(i)\, F(t; Q_i). \tag{5}$$

The KERD $P(Q_i)$ can be obtained from the coefficients $W(i)$ which give the best fit to experiment $F(t)$:

$$P(Q_i)=[W(i)/\sum_i W(i)]/[4(2n-1)E_o]. \tag{6}$$

A KERD extracted from these regression coefficients is plotted as a step graph in Fig. 8 together with the QET prediction. The QET kinetic energy release distribution $P(Q; E_i)$ to be compared to TPEPICO experiments is given to be

$$P(Q; E_i)\, dQ=\rho^{\neq}(E_i-E_a-Q)\, dQ/\, W^{\neq}(E_i-E_a). \tag{7}$$

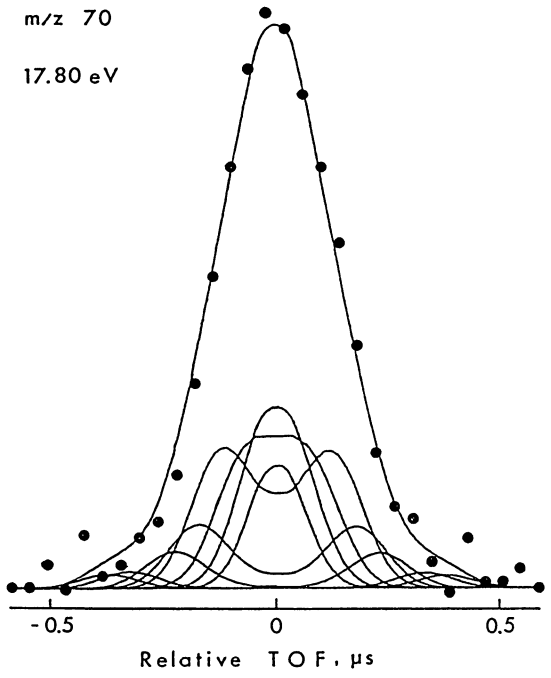

Fig. 7. An example of TOF distributions of the m/z 70 ion and a deconvolution result by the multiple linear regression method. The solid curves are the flight time distributions simulated for a series of the nine discrete kinetic energy releases and their sum to be compared with experiment.

Herein, $\rho^{\neq}(E_i-E_a-Q)$ is the state density of the transition state at internal energy of E_i-E_a-Q, and $W^{\neq}(E_i-E_a)$ is the state sum of the activated complex with excess energy E_i-E_a.

The average KERs are then obtained by

$$\langle Q\rangle_{E_i}=\int_0^{E_i-E_a} Q\, P(Q; E_i)\, dQ, \tag{8}$$

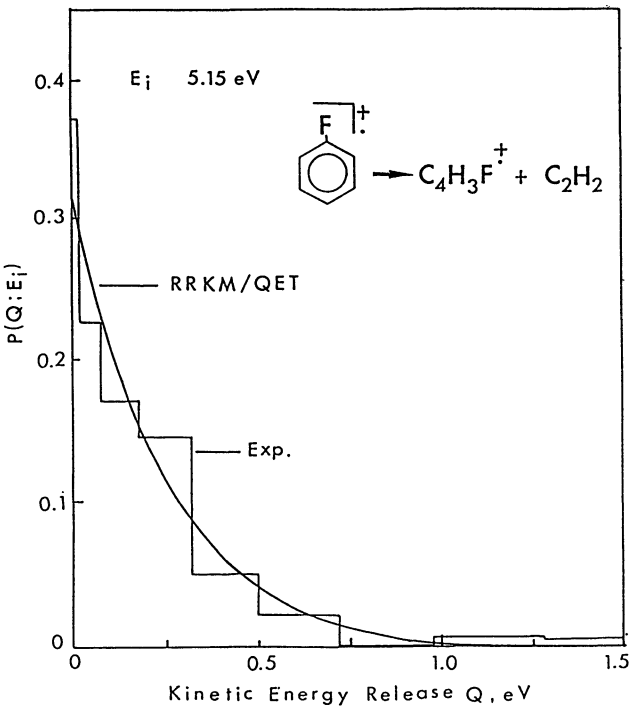

Fig. 8. A KERD for the formation of $C_4H_3F^+$ extracted from its flight time distribution is presented together with the QET prediction.

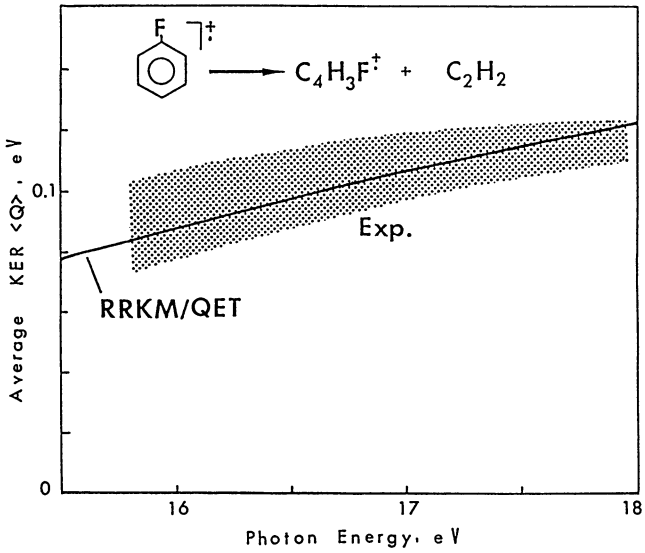

Fig. 9. Average KERs $\langle Q\rangle$ observed for the formation of $C_4H_3F^+$ (shaded area). The solid curve is the average KERs calculated by QET.

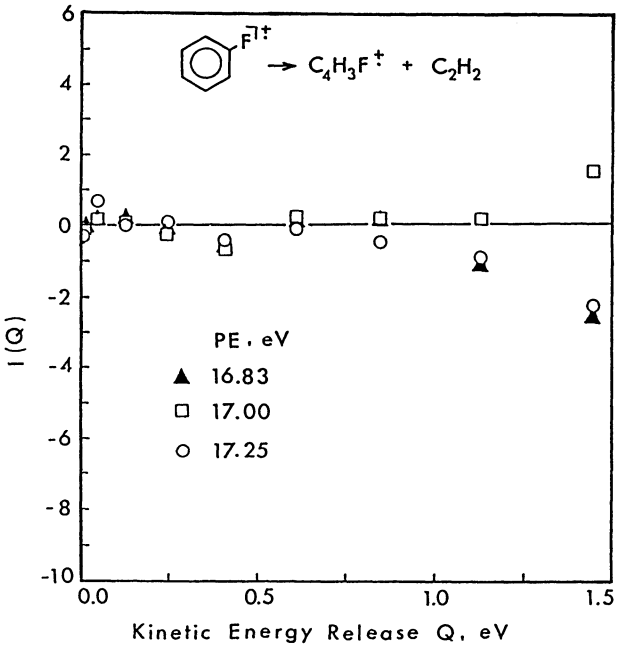

Fig. 10. Surprisal plots of KERDs observed for the $C_4H_3F^+$ formation.

and are presented in Fig. 9. Thus as seen in the figures the experimental KERDs and KERs seem to be in good agreement with the statistical expectations.

B. Surprisal Plot. Levine and Bernstein[25,26] have recently developed the thermodynamic approach to collision processes in order to bridge the gap between the equilibrium and disequilibrium on the basis of information theory. The authors[24] introduced the concept of the "surprisal" to measure how an experimental result differs from a prediction. If $P^{\circ}(Q)$ is the prior distribution with a kinetic energy release Q, the surprisal $I(Q)$ of an experimental distribution $P(Q)$ is defined as

$$I(Q) = -\ln[P(Q)/P^{\circ}(Q)]. \quad (9)$$

Here we used the QET kinetic energy release distribution as the prior distribution. The surprisal plots (Fig. 10) showed almost zero less than 0.5 eV and strongly suggest that the observed KERDs are consistent with those predicted by the statistical rate theory of mass spectra. Scattered data points over 0.5 eV corresponding to the tail of a TOF distribution are obviously due to experimental errors.

As a conclusion, whereas this molecule contains a heteroatom fluorine, statistical dissociation thus observed indicates that internal conversion controls fragmentation of the fluorobenzene ion because of its high state density.

We thank the USA Department of Energy for support of this work under Contract No. DE-AC02-76-ER02567 and the Regional Facility in Mass Spectrometry at the University of Nebraska.

References

1) H. M. Rosenstock, M. B. Wallenstein, A. L. Wharhaftig, and H. Eyring, *Proc. Natl. Acad. Sci. U.S.A.*, **38**, 667 (1952).
2) W. Frost, "Theory of Unimolecular Reactions," Academic Press, New York (1973).
3) D. L. Bunker, "Theory of Elementary Gas Reaction, Rates," Pergamon, Oxford (1967).
4) A. A. Marcus, *J. Chem. Phys.*, **20**, 359 (1952).
5) I. G. Simm, C. J. Danby, J. H. D. Eland, and P. I. Mansell, *J. Chem. Soc., Faraday Trans. 2*, **72**, 426 (1976).
6) M. G. Inghram, G. R. Hanson, and R. Stockbauer, *Int. J. Mass Spectrom. Ion Phys.*, **33**, 253 (1980).
7) T. Nishimura, G. G. Meisels, and Y. Niwa, *J. Chem. Phys.*, **91**, 4009 (1989).
8) J. H. D. Eland, "Photoelectron Spectroscopy," Butterworths, London (1974), p. 180.
9) T. Baer, in "Gas Phase Ion Chemistry," ed by M. T. Bowers, Academic Press, New York (1979), Vol. I, Chap. 5.
10) J. Dannacher, H. M. Rosenstock, R. Buff, A. C. Parr, R. L. Stockbauer, R. Bombach, and J.-P. Stadelmann, *Chem. Phys.*, **75**, 23 (1983).
11) R. Bombach, J. Dannacher, and J.-P. Stadelmann, *J. Am. Chem. Soc.*, **105**, 4205 (1983).
12) R. B. Bernstein, "Chemical Dynamics via Molecular Beam and Laser Techniques," Clarendon Press, Oxford (1982), Chap. 9.
13) C. F. Batten, J. A. Taylor, B. P. Tsai, and G. G. Meisels, *J. Chem. Phys.*, **69**, 2547 (1978).
14) C. F. Batten, J. A. Taylor, and G. G. Meisels, *J. Chem. Phys.*, **65**, 3316 (1976).
15) W. C. Wiely and I. H. McLaren, *Rev. Sci. Inst.*, **26**, 1150 (1955).
16) J. L. Franklin, P. M. Hierl, and D. A. Whan, *J. Chem. Phys.*, **47**, 3148 (1967).
17) T. Nishimura, P. R. Das, and G. G. Meisels, *J. Chem. Phys.*, **84**, 6190 (1986).
18) A. S. Werner and T. Baer, *J. Chem. Phys.*, **62**, 2900 (1975).
19) R. Bombach, J. Dannacher, and J.-P. Stadelmann, *Int. J. Mass Spectrom. Ion Proc.*, **58**, 217 (1984).
20) G. Z. Whitten and B. S. Rabinovitch, *J. Chem. Phys.*, **38**, 2466 (1963).
21) I. Powis, P. I. Munsell, and C. J. Danby, *Int. J. Mass Spectrom. Ion Phys.*, **32**, 15 (1979).
22) D. M. Mintz and T. Baer, *J. Chem. Phys.*, **65**, 2407 (1976).
23) M. L. Vestal, in "Fundamental Processes in Radiation Chemistry," ed by P. Ausloos, Interscience, New York (1968), Chap. 2.
24) R. D. Levine and R. B. Bernstein, "Molecular Reaction Dynamics," Clarendon Press, Oxford (1974).
25) I. Powis, *J. Chem. Soc., Faraday Trans. 2*, **75**, 1294 (1979).
26) C. Lifshitz, *Int. J. Mass Spectrom. Ion Phys.* **43**, 179 (1982).
27) T. P. Devies and J. W. Rabalais, *J. Electron Spectrosc. Relat. Phenm.*, **1**, 355 (1972/73).
28) A. N. H. Yeo and D. H. Williams, *Chem. Commun.*, **1970**, 886.
29) J. R. Majer and C. R. Patrick, *Trans. Faraday Soc.*, **58**, 17 (1962).
30) J. R. Majer and C. R. Patrick, *Adv. Mass Spectrom.*, **2**,

555 (1963).
31) J. Momigny, *Bull. Soc. R. Sci. Liége,* **28**, 251 (1959).
32) I. Howe and D. H. Williams, *J. Am. Chem. Soc.,* **91**, 7137 (1969).
33) L. M. Sverdlov, M. A. Kovner, and E. P. Krainov, "Vibrational Spectra of Polyatomic Molecules," John Wiely & Sons, New York (1974), p. 448.
34) H. M. Rosenstock, K. Draxl, B. W. Steiner, and J. H. Herron, *J. Phys. Chem. Ref. Data,* **6**, Supplement 1 (1977), p. I-146.